ADVANCES IN ATMOSPHERIC SCIENCES, VOL. 30, NO. 6, 2013, 1507–1525

Remote Effects of Tropical Cyclone Wind Forcing over the Western Pacific on the Eastern Equatorial Ocean

ZHANG Rong-Hua*[1,2] (张荣华), PEI Yuhua[1,3] (裴玉华), and CHEN Dake[1] (陈大可)

[1] *State Key Laboratory of Satellite Ocean Environment Dynamics, the 2nd Institute of Oceanography, State Oceanic Administration, Hangzhou* 310012

[2] *Earth System Science Interdisciplinary Center, University of Maryland, Maryland, USA*

[3] *College of Physical and Environmental Oceanography, Ocean University of China, Qingdao* 266003

(Received 27 November 2012; revised 5 February 2013; accepted 4 March 2013)

ABSTRACT

An ocean general circulation model (OGCM) is used to demonstrate remote effects of tropical cyclone wind (TCW) forcing in the tropical Pacific. The signature of TCW forcing is explicitly extracted using a locally weighted quadratic least-squares regression (called as LOESS) method from six-hour satellite surface wind data; the extracted TCW component can then be additionally taken into account or not in ocean modeling, allowing isolation of its effects on the ocean in a clean and clear way. In this paper, seasonally varying TCW fields in year 2008 are extracted from satellite data which are prescribed as a repeated annual cycle over the western Pacific regions off the equator (poleward of 10°N/S); two long-term OGCM experiments are performed and compared, one with the TCW forcing part included additionally and the other not. Large, persistent thermal perturbations (cooling in the mixed layer (ML) and warming in the thermocline) are induced locally in the western tropical Pacific, which are seen to spread with the mean ocean circulation pathways around the tropical basin. In particular, a remote ocean response emerges in the eastern equatorial Pacific to the prescribed off-equatorial TCW forcing, characterized by a cooling in the mixed layer and a warming in the thermocline. Heat budget analyses indicate that the vertical mixing is a dominant process responsible for the SST cooling in the eastern equatorial Pacific. Further studies are clearly needed to demonstrate the significance of these results in a coupled ocean-atmosphere modeling context.

Key words: tropical cyclone wind forcing, ocean modeling, remote effects, ocean pathway, satellite data

Citation: Zhang, R.-H., Y. H. Pei, and D. K. Chen, 2013: Remote effects of tropical cyclone wind forcing over the western Pacific on the eastern equatorial ocean. *Adv. Atmos. Sci.*, **30**(6), 1507–1525, doi: 10.1007/s00376-013-2283-0.

1. Introduction

Tropical cyclones (TCs) exert strong wind forcing to the ocean. Previously, local responses of the ocean have been extensively investigated (e.g., Price, 1981; Jacob et al., 2000; Ginis, 2002; Lin et al., 2003; Price et al., 2008; Huang et al., 2009; Zedler, 2009; Vincent et al., 2012). Recently, remote effects of TC-induced wind forcing on large-scale ocean state and low-frequency climate variability have been of an increased interest as debates continue about the relationships between TC activity and global warming. For example, it has been illustrated that small-scale and short-lived TCs can be of climatic and global importance, including their remote influences on heat transport and thermal conditions (e.g., Emanuel, 1987, 2001; Henderson-Sellers et al., 1998; Webster et al., 2005; Chen et al., 2006; Pasquero and Emanuel, 2008; Korty et al., 2008; Hu and Meehl, 2009; Jansen and Ferrari, 2009; Chen and Tam, 2010).

The tropical Pacific is the home to the El Niño-Southern Oscillation (ENSO), the largest interannual variability signal having significant effects on weather and climate worldwide (e.g., Zhang et al., 2013), in-

*Corresponding author: ZHANG Rong-Hua, rzhang@essic.umd.edu

cluding TCs. For example, as examined by numerous studies, ENSO is one major factor impacting TC frequency, genesis, intensity, and tracks over the tropical Pacific on interannual time scales (e.g., Chan, 1985, 2000; Irwin and Davis, 1999; Chia and Ropelewski, 2002; Wang and Chan, 2002; Elsner and Liu, 2003; Camargo and Sobel, 2005; Chen et al., 2006; Camargo et al., 2007). The western Pacific is one of the most active regions for TC genesis and intensification. Local perturbations induced by tropical cyclone wind (TCW) forcing to the ocean can be large, including enhanced mixing in the upper ocean and changes in the vertical thermal structure. While conditions disturbed by TCs in the atmosphere can be restored very quickly (a couple of days) after TCs leave away, those in the ocean can persist weeks and longer, characterized by a cooling in the mixed layer (ML) and a warming beneath the ML and in the thermocline. These large, persisted thermal perturbations tend to evolve slowly around the ocean basin, potentially having effects on remote areas where TCW forcing is not directly felt. Additionally, the induced perturbations in remote regions can trigger local processes that, in turn, may further enhance the related presponses. Some evidence has been presented for remote influences that TCW forcing may exert on thermal conditions in the Pacific (e.g., Sriver and Huber, 2007, 2010; Fedorov et al., 2010; Sriver et al., 2010; Kim et al., 2011).

This work aims to explore the possible feedbacks of TC-induced wind forcing onto large-scale ocean state and low-frequency coupled ocean-atmosphere variability in the tropical Pacific. While ENSO has been demonstrated to modulate TC activities over the western tropical Pacific, the possible effects of TC activities on ENSO are poorly understood. Here we seek any connection of thermal anomalies between the western tropical Pacific (where TCs are mostly active with large thermal anomalies induced locally in the ocean) and the eastern equatorial Pacific (where changes in SSTs are critically important to ENSO). To this end, an ocean general circulation model (OGCM) and satellite wind data are utilized to illustrate remote effects of TCW forcing over the western tropical Pacific on oceanic conditions in the eastern equatorial region. Some specific questions are going to be investigated. To what extent can TCW forcing over the western tropical Pacific remotely affect the ocean in the east? What are the characteristics of the remote responses of the ocean in the east to TCW forcing in the west? What processes are involved in such remote effects?

The paper is organized as follows. Section 2 briefly describes an OGCM, satellite data and the locally weighted quadratic least-squares regression (LOESS) method used to extract TCW forcing fields, and modeling experiment design. Section 3 deals with TCW-induced forcing effects on ocean simulations by comparing a reference TCW run and a no-TCW run, including analyses of the mixed layer heat budget and of potential processes responsible for the effects on SST. In section 4, additional experiments are further performed to illustrate the sensitivity to some parameters representing TCW forcing intensity. A conclusion and discussion are given in section 5.

2. Models and data

Figure 1 displays a modeling system used in this work, consisting of a basin-scale OGCM of the tropical Pacific and TC-induced wind (TCW) forcing component which can be explicitly represented over the western tropical Pacific. In this ocean-only modeling context, the total wind stress (τ) can be separated into its climatological part ($\tau_{\rm clim}$) and TC-induced part ($\tau_{\rm TC}$). In this section, we briefly describe these various components and experiment designs.

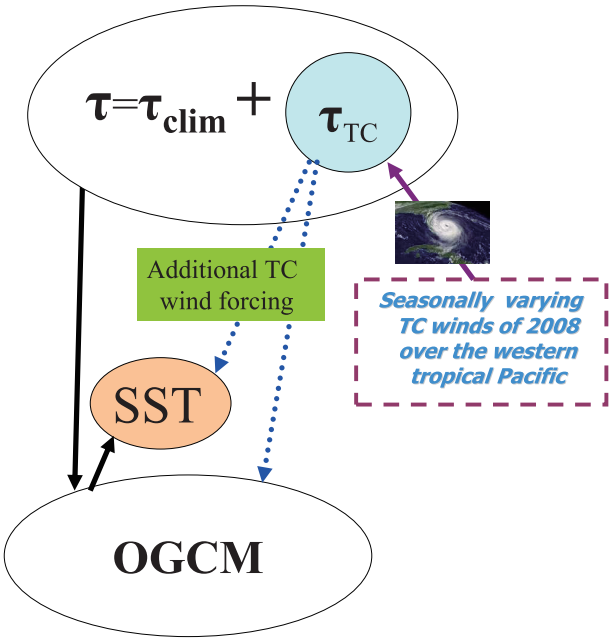

Fig. 1. A schematic diagram showing a basin-scale ocean model of the tropical Pacific, with TC-induced wind forcing explicitly taken into account. The total wind stress used to force the ocean is separated into its climatological part ($\tau_{\rm clim}$) and TC part ($\tau_{\rm TC}$), written as: $\tau = \tau_{\rm clim} + \alpha_{\rm TC} \times \tau_{\rm TC}$. The former is prescribed from observed long-term climatology; the latter can be explicitly extracted from satellite data using the LOESS method. The extracted $\tau_{\rm TW}$ field is then added onto the prescribed $\tau_{\rm clim}$ field to force the OGCM. As such, the TC wind part can be conveniently switched on or off in ocean modeling to represent its forcing effects.

2.1 *An ocean general circulation model*

The OGCM used in this work is the reduced gravity, primitive equation, sigma-coordinate model developed by Gent and Cane (1989). The vertical structure of the ocean model consists of a mixed layer (the first layer) and a number of layers below which are specified according to a sigma-coordinate. The mixed layer depth and the thickness of the last sigma layer are calculated prognostically. Several related efforts have been devoted to improving this ocean model significantly. Chen et al. (1994) developed a hybrid mixed layer model which is explicitly embedded into the OGCM. Murtugudde et al. (1996) incorporated an advective atmospheric mixed layer (AML) model into the OGCM to estimate sea surface heat fluxes and take into account a non-local effect on SST induced by the atmospheric boundary layer. This heat flux parameterization allows a realistic representation of the feedbacks between mixed layer depths, SSTs, and the surface heat fluxes (e.g., Seager et al., 1995). Complete hydrology was added to the model that represents freshwater flux as a natural boundary condition (Murtugudde and Busalacchi, 1998). Additionally, the effect of penetrative radiation on the upper tropical ocean circulation was taken into account, with attenuation depth ($H_{\rm p}$) derived from satellite ocean color data (Murtugudde et al., 2002). These process-oriented studies have improved simulations of ocean circulation and thermal structure significantly. More recent efforts with this OGCM include the developments of a hybrid coupled ocean-atmosphere model (HCM) for the tropical Pacific (Zhang et al., 2006); the developed HCM has been used to understand tropical instability waves-induced wind feedback, freshwater flux-induced feedback, and ocean biology-induced feedback within the tropical Pacific climate system (Zhang and Busalacchi, 2008, 2009; Zhang et al., 2009, 2012), respectively.

The OGCM domain covers the tropical Pacific basin from 124°E to 76°W and from 25°S to 25°N, having horizontal resolution of 1° (lon)×0.5° (lat), and 31 layers in the vertical. Near the model southern and northern boundaries (poleward of 20°S/N), sponge layers are imposed. The OGCM is initiated from the WOA01 temperature and salinity fields (Levitus et al., 2005), and is integrated for 20 years (the spinup run) using prescribed monthly-mean climatological atmospheric forcing fields, including the reanalysis wind stress fields from the European Center for Medium-Range Weather Forecasts (ECWMF) averaged from 1985 to 1998 (e.g., Hackert et al., 2001), solar radiation from the Earth Radiation Budget Experiment (ERBE), cloudiness from the International Satellite Cloud Climatology Project (ISCCP), and precipitation from Xie and Arkin (1995). The surface heat flux for the OGCM is interactively calculated using the Seager et al. (1995) AML model; no relaxation of SST to observations is taken in any OGCM simulation performed in this study. Note that the OGCM is forced by monthly-mean climatological atmospheric fields prescribed on 2°×2° spatial grids, which are interpolated onto the ocean model grid and model time steps. As such, TCW forcing component is completely excluded in the prescribed climatological atmospheric forcing fields, but can be explicitly added in ocean simulations using satellite wind data and the LOESS method described below.

2.2 *Satellite observations and the LOESS method used to extract TCW forcing field*

Satellite data are used for our TCW-related analyses and modeling studies. Wind data are from the Cross-Calibrated, Multi-Platform (CCMP) satellite scatterometer wind product (Atlas et al., 2011); SST data are from the Tropical Rainfall Measuring Mission (TRMM) microwave imager (TMI; Wentz et al., 2000). The horizontal grid of these satellite data has a resolution of 0.25°×0.25° in space and six-hour sampling in time.

High space-time resolution satellite winds from the CCMP data include various forcing signals to the ocean, which are of different origins, including the Madden Julian Oscillations (MJOs), tropical instability waves (TIWs), the westerly wind burst, and TCs etc. If these raw wind data are directly used to force an ocean model, various wind forcing signals with different physical origins are mixed up, leading to their effects on the ocean that are lumped together and difficult to isolate from each other. Here, we seek a way by which TCW forcing fields can be explicitly extracted from spatially varying large-scale background wind fields, which can then be additionally included in ocean modeling to isolate its forcing effect on the ocean.

To this end, a locally weighted quadratic least-squares regression (LOESS) method is utilized (e.g., O'Neill et al., 2010). Specifically, a smoothed value ($\overline{A}$) of a field (A) at a grid point can be estimated by fitting a regression surface to some subset data locally. Then, a perturbation field is obtained as $A' = A - \overline{A}$. As is shown in O'Neill et al. (2010), the resultant perturbation fields depend on the so-called half span parameters in the LOESS method [denoted as α_x and α_y in the zonal (x) and meridional (y) directions], which indicate how much of subset data is used to fit each quadratic regression locally. The larger the values of α_x and α_y, the smoother the $\overline{A}$ field, and the stronger the perturbation fields (A'), respectively.

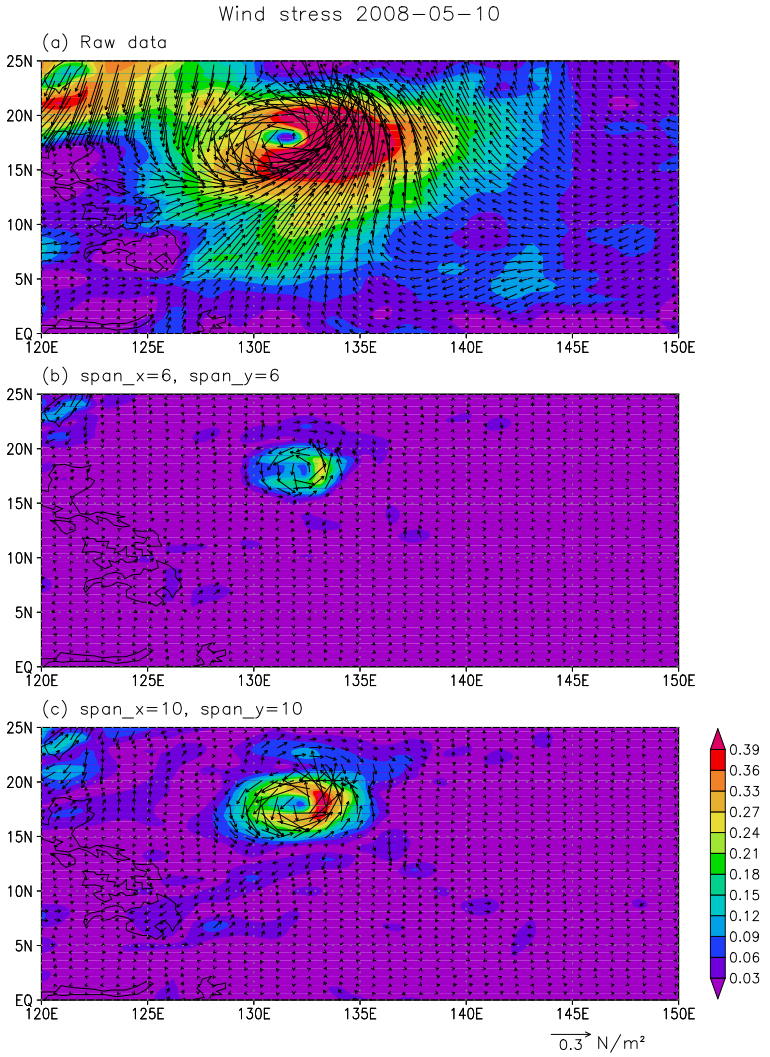

Fig. 2. Wind stress fields from the satellite measurements: the original daily fields on 10 May 2008 (a), and the TC-related perturbation part extracted using the LOESS method with half-span smoothing parameters in the zonal (x) and meridional (y) directions: $\alpha_x = 6^\circ$ and $\alpha_y = 6^\circ$ (b), and $\alpha_x = 10^\circ$ and $\alpha_y = 10^\circ$ (c), respectively. As shown, the structure and amplitude of the derived TCW field are sensitive to the values of α_x and α_y. For example, when taking $\alpha_x = 6$ and $\alpha_y = 6$, the structure of TC wind forcing can be well represented, but the amplitude is underestimated.

An example is illustrated in Fig. 2 for TC-induced wind stress fields on 10 May 2008, which are extracted using the LOESS method from original satellite data; here a 2-D LOESS filter is applied to daily-mean wind stress fields in the zonal and meridional directions. It is seen that the amplitude and structure of the resultant TC-related perturbation fields are sensitive to the half-span parameters taken in the zonal and meridional directions (i.e., α_x and α_y). When taking $\alpha_x = 6^\circ$ and $\alpha_y = 6^\circ$, the structure of the TCW fields can be clearly depicted from spatially varying background wind fields, but the amplitude and spatial extent are underestimated. When taking $\alpha_x = 10^\circ$ and $\alpha_y = 10^\circ$, TCW fields can be represented reasonably well. Note that the use of the LOESS method is intended to explicitly extract TCW forcing structure from spatially varying background wind fields; then the derived TCW pattern can be additionally combined with other wind forcing components to drive ocean models. As such, the TCW forcing component can be conveniently switched on or off in ocean-only modeling experiments (Fig. 1), allowing its effects to

be represented and compared in a clean and clear way.

2.3 *Experiment designs*

Figure 3 illustrates the TC tracks observed in year 2008 over the Pacific basin (Chu et al., 2002). It is seen that the western Pacific is one of the most active regions for TC genesis and intensification. As TCs are generated in the atmosphere, they induce quick and large responses in the ocean. The induced thermal perturbations tend to persist in the ocean for weeks and longer, potentially exerting a remote influence on the ocean basinwide. While local oceanic responses to TC-induced wind forcing in the western tropical Pacific are well simulated and understood (e.g., TC-induced mixing effects on the upper ocean, which are characterized by cooling in the mixed layer and warming in the thermocline), its remote effects on oceanic thermal structure in the eastern equatorial Pacific have not been convincingly demonstrated. To identify any connection between TC activities over the western Pacific and thermal responses in the eastern equatorial Pacific, TCW forcing is taken into account only over the western region as follows.

In an ocean-only modeling context, the total wind stress (τ) fields used to force the OGCM is written as (Fig. 1): $\tau = \tau_{\rm clim} + \alpha_{\rm TC} \times \tau_{\rm TC}$, where $\tau_{\rm clim}$ is a prescribed climatological wind stress part, $\tau_{\rm TC}$ is TC-induced wind forcing part, and $\alpha_{\rm TC}$ is a scalar parameter introduced to represent the strength of TCW forcing. As detailed above, the TCW forcing part is explicitly extracted from six-hour satellite data using the LOESS method with $\alpha_x = 6^\circ$ and $\alpha_y = 6^\circ$; the derived $\tau_{\rm TC}$ part is then added onto the $\tau_{\rm clim}$ fields to force the OGCM. In addition, the introduced $\alpha_{\rm TC}$ parameter can be utilized to rescale the $\tau_{\rm TC}$ intensity (i.e., the $\tau_{\rm TC}$ fields derived from the LOESS method are multiplied by this parameter so that its intensity can be matched to what is observed in nature).

As observed, TCs exhibit strong seasonal variations over the western Pacific, being mostly active in May–September. To take into account TC-induced seasonally modulating effects on ocean simulations, six-hour varying $\tau_{\rm TC}$ data during January–December from one full year, arbitrarily chosen in year 2008, are taken to form a temporal succession fields for a repeated annual cycle, which are interpolated to model time step and combined with $\tau_{\rm clim}$ to force the OGCM (i.e., both $\tau_{\rm clim}$ and $\tau_{\rm TC}$ fields are prescribed as a repeated annual cycle in model time integration). Note that when the $\tau_{\rm TC}$ part is extracted from original satellite wind data using the LOESS method, its annual mean at each spatial grid (averaged over a full year using six-hour varying $\tau_{\rm TC}$ fields), $\overline{\tau}_{\rm TC}$, can be nonzero, which can induce a mean bias when it is used to force an OGCM, potentially contaminating the effect assessments associated with TCW forcing. To avoid this problem, the annual-mean value, $\overline{\tau}_{\rm TC}$, is removed at each spatial grid and the resultant ($\tau_{\rm TC} - \overline{\tau}_{\rm TC}$) fields are actually used in ocean modeling experiments.

In this paper, we examine remote effects of TCW forcing over the western Pacific on thermal conditions in the eastern equatorial region. The $\tau_{\rm TC}$ forcing is applied only to the western tropical North and South Pacific regions (to the regions west of 170°E, and pol eward of 10°N and 10°S, respectively); outside these $\tau_{\rm TC}$ forcing regions, $\tau_{\rm TC}$ is set to be zero. Figure 4 indicates the structure and amplitude of $\tau_{\rm TC}$ calculated from year 2008 using six-hour varying data. Over the

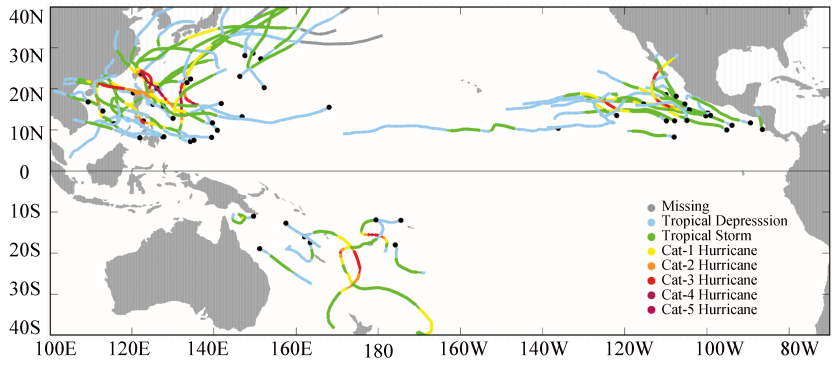

Fig. 3. An example of TC genesis and tracks observed in year 2008 over the Pacific basin. Active TC regions include the Northwestern (NW) tropical Pacific, the Southwestern (SW) tropical Pacific, and the Northeastern (NE) tropical Pacific. In the ocean modeling performed in this paper, 6-h varying TCW fields of the year 2008 are explicitly extracted from satellite data and are then prescribed over the western Pacific to represent its forcing effects on the ocean.

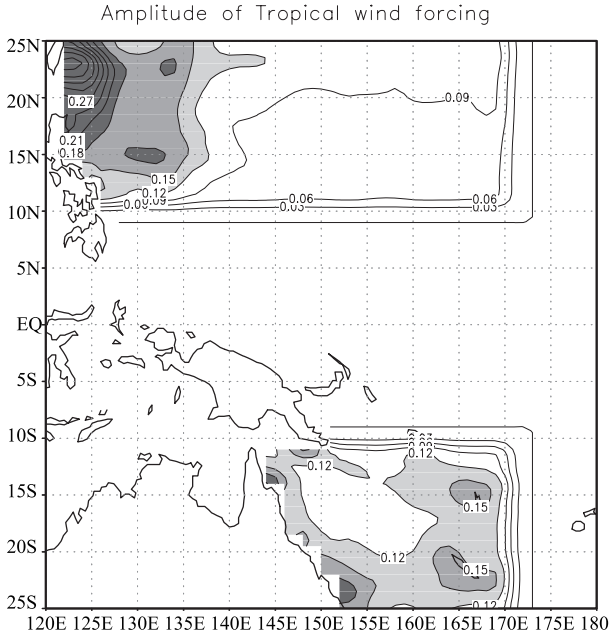

Fig. 4. The amplitude of the standard deviation of zonal and meridional TC-induced wind stress components, calculated from 6-hour varying perturbation fields in year 2008 which are extracted using the LOESS filtering method with $\alpha_x = 6$ and $\alpha_y = 6$. The contour interval is 0.03×10^{-5} N cm^{-2}.

TC active regions in the western tropical Pacific, the amplitude of the $\tau_{\rm TC}$ part is about 10%–20% of that of the prescribed annual-mean climatological wind stress. In addition, the regions with large $\tau_{\rm TC}$ amplitude correspond well to the major TC tracks over the western tropical Pacific as shown in Fig. 3.

Two experiments are performed using the OGCM (Fig. 1), which is started from the same spinup run. One is referred to a no-TCW run in which the $\tau_{\rm TC}$ part is not included ($\alpha_{\rm TC} = 0.0$); another is referred to a reference TCW run, in which the $\tau_{\rm TC}$ part (taking $\alpha_{\rm TC} = 2.0$ and $\alpha_x/\alpha_y = 6^\circ$ when using the LOESS method to extract $\tau_{\rm TC}$) is explicitly incorporated into a forced OGCM simulation, with other model settings being kept exactly the same as in the no-TCW run. The OGCM is integrated for 11 years for both runs (arbitrarily denoted as being from year 1 to year 11), in which an equilibrium ocean state is reached. Note that in the TCW run, the six-hour varying annual cycle derived in year 2008 is repeatedly applied to the 11-year OGCM simulations. In this way, seasonally modulated effects of $\tau_{\rm TC}$ on the ocean are taken into account in the ocean modeling (e.g., TCs are mostly active in May–September). In the following, the differences in monthly-mean outputs between the two runs in the last year (year 11) are calculated to represent long-term effects induced by the TCW forcing. Also note that the $\tau_{\rm TC}$ part is derived from year 2008, which is arbitrarily chosen to represent a typical condition of TC activity over the western Pacific. Further sensitivity experiments are also performed with varying values of $\alpha_{\rm TC}$, α_x and α_y to illustrate the relationships between the TCW forcing intensity and the corresponding ocean responses.

3. Remote effects on thermal conditions in the eastern equatorial Pacific

The prescribed TCW forcing over the western Pacific induces large perturbations to the ocean locally, characterized by a cooling in the mixed layer (ML), and a warming beneath the ML and in the thermocline (e.g., Figs. 5–6). These induced thermal perturbations (the surface cooling and subsurface warming signals) persist in the ocean for weeks and longer, which tend to propagate away from the source forcing regions into other remote areas where no TCW forcing is directly imposed, acting to exert non-local influences on the ocean conditions basinwide. In particular, thermal responses are remotely seen in the eastern equatorial Pacific where the thermocline is shallow, and the oceanic mixing and upwelling are strong. Some detailed analyses are given in this section.

3.1 *Annual mean fields and seasonal variations*

Figures 5–8 illustrate the horizontal and vertical distributions of some selected annual mean fields simulated from the no-TCW run and TCW run. When the TCW forcing is imposed over the western Pacific, a large-scale cooling pattern emerges in the eastern equatorial Pacific. For example, relative to the no-TCW run, a systematic cooling effect on SST in the TCW run is evident over the eastern and central equatorial Pacific: negative SST differences between these two runs can be as large as 0.3°C (Fig. 5c). As shown in Fig. 6 for the vertical structures of temperature differences, the cooling is seen to extend down to the upper thermocline, accompanied with a warming in the thermocline. Thus, the vertical temperature gradient between the mixed layer and the thermocline in the TCW run is reduced over the eastern equatorial Pacific, which leads to changes in the vertical density distribution, acting to de-stabilize the stratification and enhance the vertical mixing in the upper ocean.

Other oceanic fields also show systematic and coherent differences. For example, accompanied with the negative SST difference, a positive heat flux is seen from the atmosphere to the ocean at the sea surface over the eastern equatorial Pacific (Fig. 7). Further analyses indicate that the differences in the total heat

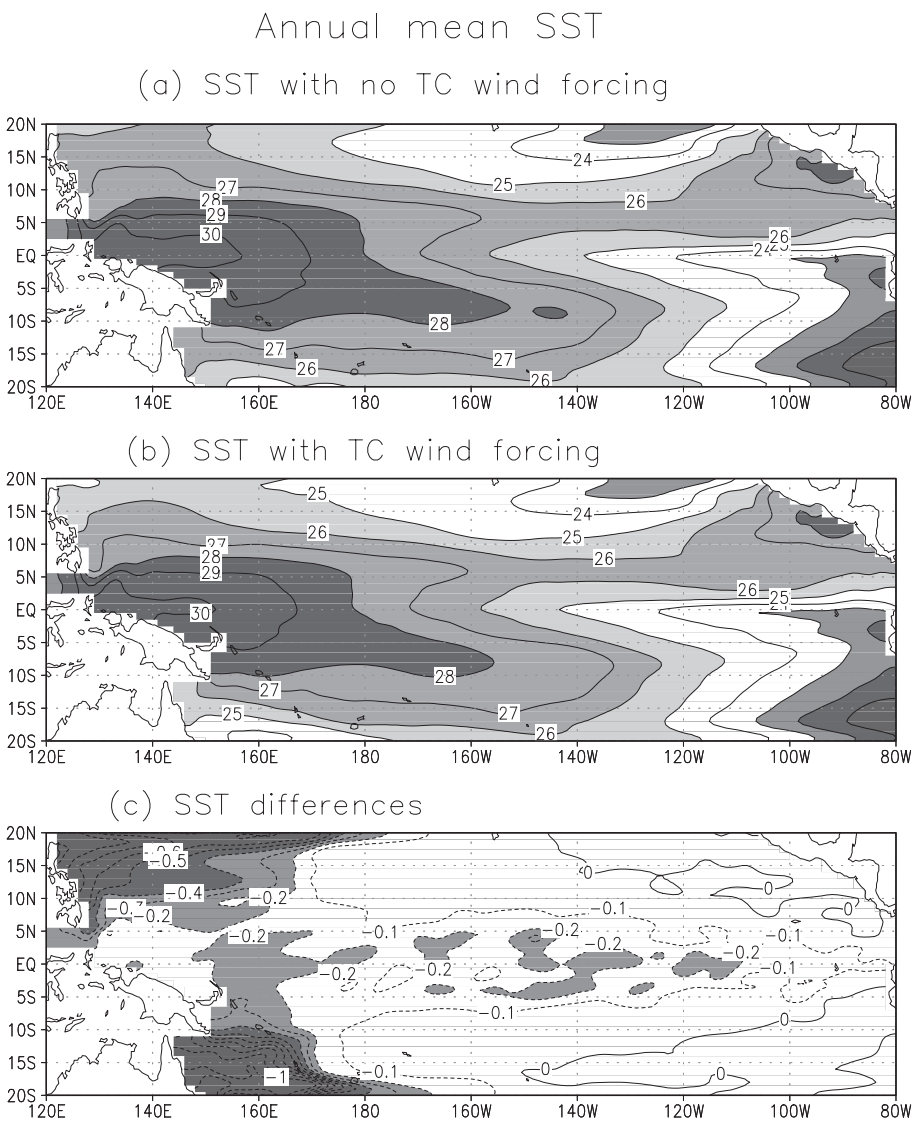

Fig. 5. Annual-mean SST fields simulated in the no-TCW run (a) and reference TCW run (b), and their differences (c; the reference TCW run minus no-TCW run), respectively. The contour interval is 1°C in (a) and (b), and 0.1°C in (c).

flux are mostly attributed to the latent heat flux effect (figures not shown). The negative correlations between the TCW forcing-induced heat flux and SSTs in the eastern equatorial Pacific indicate that the surface heat flux response acts to have a damping effect on SST; thus, the cooling in the upper ocean should be attributed to ocean processes (see the analyses below).

While the differences in the sea surface heat flux are negatively related with SSTs, those in the mixed layer depth (MLD) are of the same sign with SSTs (Fig. 8). As indicated in Fig. 8a, the mean structure of the MLD is well simulated in the no-TCW run compared with the corresponding observed fields (e.g., Monterey and Levitus, 1997). When TCW is explicitly included over the western tropical Pacific, the depth of the mixed layer is reduced in the eastern equatorial Pacific (Fig. 8b), with its annual-mean differences being 2 meter at 110°W on the equator. Note that the mixed layer depth is treated as a prognostic field in the OGCM, which is explicitly computed using a bulk mixed model (Chen et al., 1994). This model configuration allows for differentiation of even a few meters in mixed layer depth between the TCW run and no-TCW run, respectively.

Figures 9–10 further exhibit the seasonal cycles of SST, MLD and heat flux along the equator. It is seen that seasonal variations simulated in the no-TCW run are well matched with the corresponding observations.

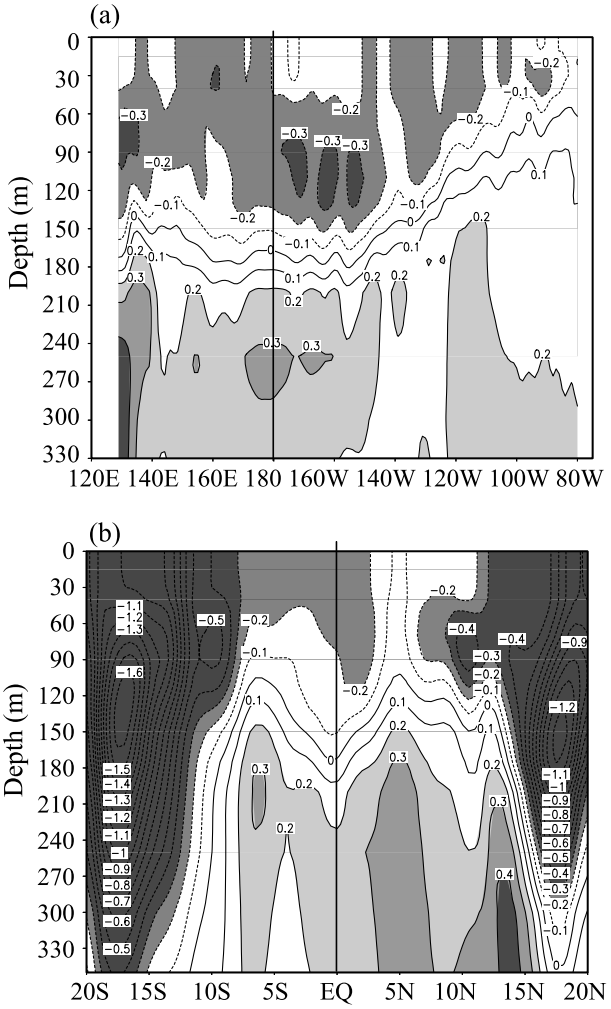

Fig. 6. Zonal-vertical section along the equator (a) and meridional-vertical section along 160°E (b) of annual-mean temperature differences between the reference TCW run ($\alpha_{TC} = 2.0$) and no-TCW run ($\alpha_{TC} = 0.0$). The contour interval is 0.1°C.

For example, the seasonal cycles of the MLD (Fig. 10a) are well depicted as compared with those observed (e.g., Monterey and Levitus, 1997). When the ocean is additionally imposed to the TCW forcing over the west, SSTs exhibit a systematic and coherent modulation to its seasonal cycles in the central and eastern equatorial Pacific: a cooling response of SST (Fig. 9a) is accompanied with a positive heat flux into the ocean (Fig. 9b) and a shoaling of the mixed layer (Fig. 10b), respectively. The peak values of the differences take place at 110 °W on the equator in January–February, being as large as −0.5°C for SST, 10 W m^{-2} for heat flux, and 10 meters for MLD. Although TC-induced wind forcing is of small scale, the resultant monthly-mean difference fields are of large scale, with one overwhelming sign in most of the eastern equatorial Pacific. Since there is no directly imposed TCW forcing over the eastern equatorial domain, the differences in the two runs are attributed to ocean processes responding to the TCW forcing prescribed over the western tropical Pacific in a remote manner.

3.2 *Oceanic processes contributing to the SST budget in the east*

To further understand oceanic processes by which the negative SST differences between the two runs are produced in the eastern equatorial Pacific, a heat budget analysis is performed for the mixed layer. In the Gent-Cane OGCM used here, the vertical entrainment/detrainment fields at the base of the ML are calculated using a bulk ML model; the vertical mixing, primarily associated with the entrainment/detrainment, is estimated using a hybrid mixing scheme (Chen et al., 1994). In addition, a background vertical diffusion effect is explicitly taken into account, but is small in magnitude. Note that as the mixed layer depth is a prognostic variable in the OGCM, all the SST budget terms are simultaneously modulated by changing depth of the ML. In the model integration, all the SST budget terms are explicitly saved at each timestep, which are then averaged to get their daily and further their monthly mean fields for analyses. In the following, the heat budget analyses are performed using monthly mean climatological fields from the model integration of the last year (i.e., the 11th year).

Figures 11–12 display the seasonal variations of the vertical mixing/advection and meridional advection along the equator in the no-TCW run; the amplitude of the zonal advection is relatively small (figures not shown). Similar to previous studies (e.g., Kessler et al., 1998), the dominant terms contributing to the SST budget in the eastern equatorial Pacific are vertical mixing/advection at the base of the ML and meridional advection. The former tends to have a cooling effect on SST (Fig. 11a), and the latter acts to have a warming one (Fig. 12a); their combined effects result in a cooling that is balanced by the heat flux at the sea surface (e.g., Fig. 7a). Seasonally, the vertical mixing cooling is largest in winter seasons (Fig. 11a), while the meridional advection warming is at maximum in September–October (Fig. 12a).

The imposed TCW forcing over the western Pacific is found to induce a modulation to the SST budget in the eastern equatorial Pacific, as represented in Figs. 11–12 for the seasonal differences between the two runs, and in Fig. 13 for the horizontal distributions of annual-mean differences in some selected budget terms. Besides the directly forced region in the western Pacific, the eastern equatorial Pacific is a reg-

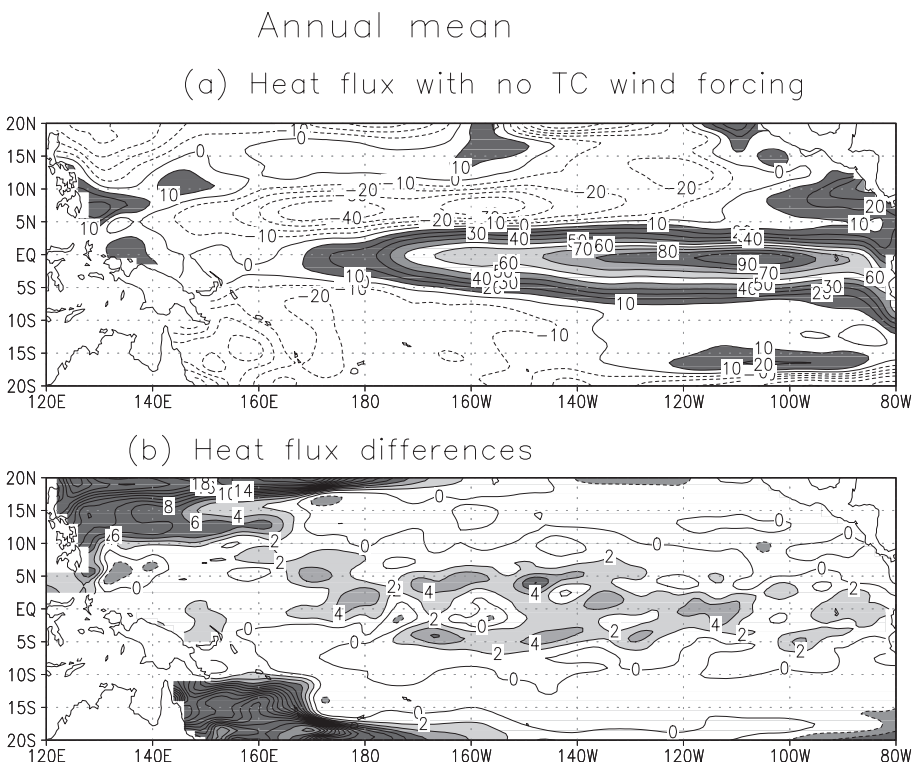

Fig. 7. Annual-mean surface heat flux calculated in the no-TCW run (a), and the differences (b) between the reference TCW run and no-TCW run. The contour interval is 10 W m^{-2} in (a) and 2 W m^{-2} in (b).

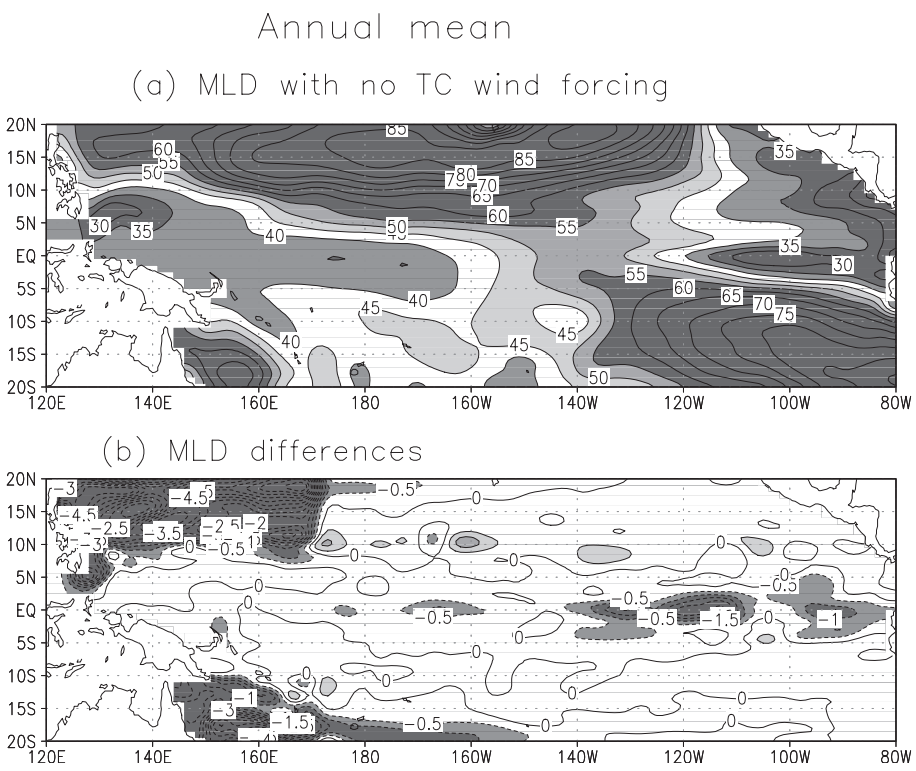

Fig. 8. Annual-mean MLD simulated in the no-TCW run (a), and the differences (b) between the reference TCW run and no-TCW run. The contour interval is 5 m in (a) and 0.5 m in (b).

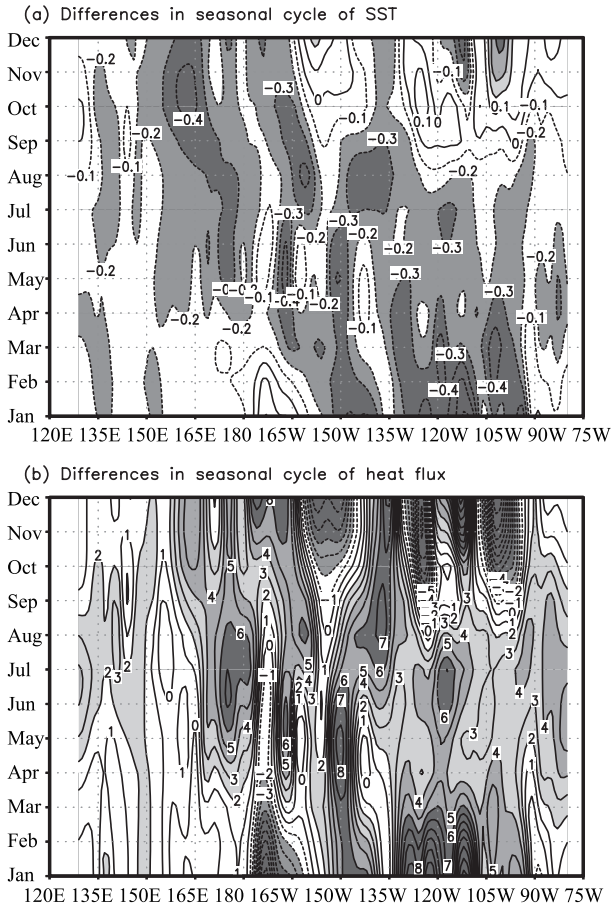

Fig. 9. Differences in the seasonal cycle of SST (a) and of surface heat flux (b) between the reference TCW run and no-TCW run along the equator. The contour interval is 0.1°C in (a) and 1 W m^{-2} in (b).

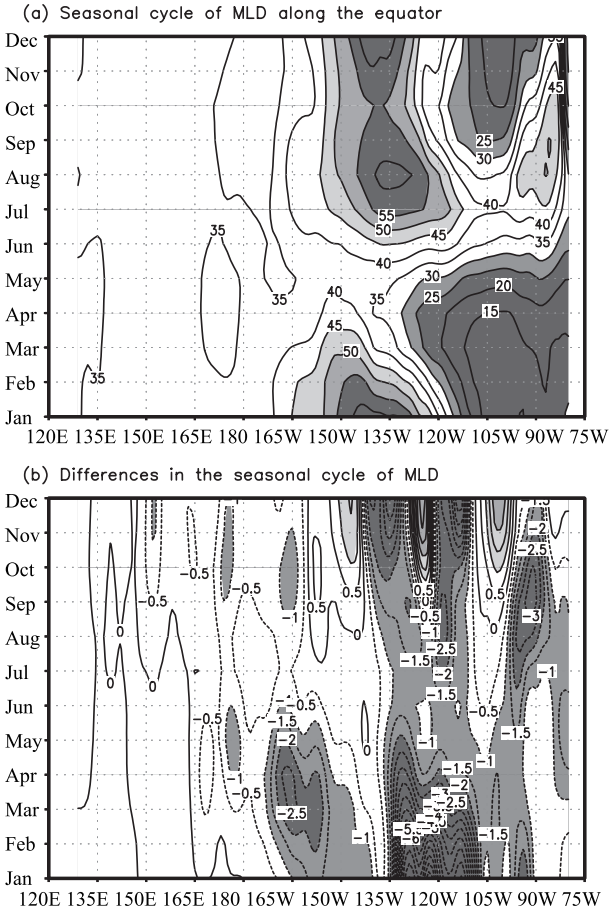

Fig. 10. Seasonal variations of MLD along the equator in the no-TCW run (a), and its differences (b) between the reference TCW run and no-TCW run. The contour interval is 5 m in (a) and 0.5 m in (b).

ion where the heat budget terms are modulated by TCW in a systematic and coherent way. Furthermore, it is seen that the vertical mixing (Fig. 11b) and meridional advection (Fig. 12b) are the two terms that are dominantly affected by the TCW forcing. When TCW forcing is taken into account in the TCW run, the cooling effect from the vertical mixing tends to be enhanced (Fig. 11b); the warming effect from the meridional advection is mostly enhanced (Fig. 12b), with their effects being compensated for by each other. The combined effects (the enhanced cooling due to the vertical mixing and increased warming due to the meridional advection) result in a net cooling tendency, which is largely balanced by a positive heat flux into the ocean at the sea surface (e.g., Fig. 9b). As these budget terms collectively give rise to a net cooling effect on SST (Fig. 13c), the resultant SST differences between the TCW run and no-TCW run are negative over the eastern equatorial Pacific, leading to a large-scale cooling pattern.

Thus, TCW forcing prescribed over the western Pacific only tends to induce a coherent remote response in the eastern equatorial Pacific, characterized by a La Niña-like pattern: a cooling of SST (Fig. 9a) is accompanied by a positive sea surface heat flux into the ocean (Fig. 9b), and a shoaling of the mixed layer (Fig. 10b) in most of the eastern equatorial region. The budget analyses indicate that the vertical mixing is a major contributor (Fig. 11b), while the surface heat flux response acts to dampen the ocean process-induced negative SST perturbation. The spatial scale of the perturbed fields in the ocean is much larger than that of the prescribed TCW forcing. While the prescribed TCW forcing has zero annual-mean, the induced annual-mean differences in SST, heat flux and MLD are not zero both in the western and the eastern equatorial Pacific, illustrating a rectified influence on the large-scale ocean state exerted by small-scale and

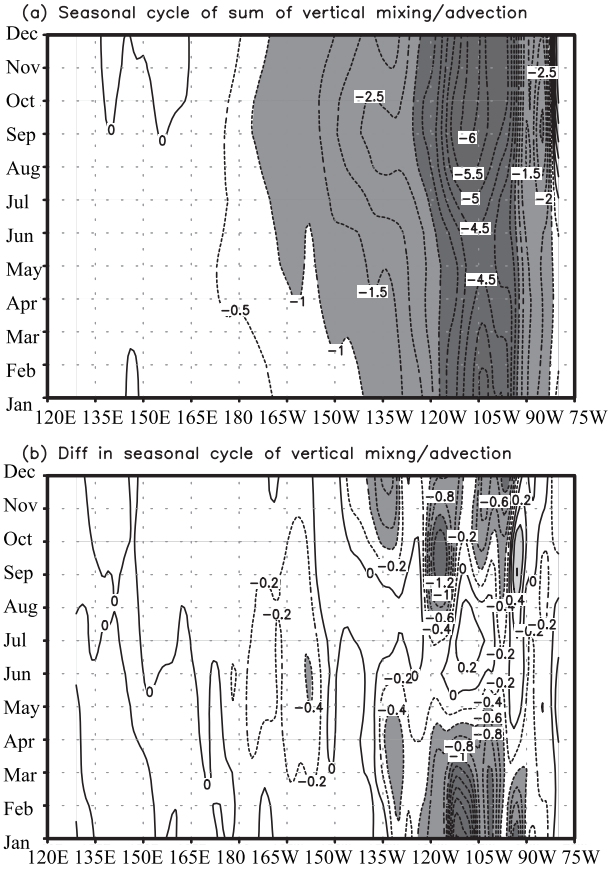

Fig. 11. Seasonal variations of the sum of vertical mixing and advection along the equator in the no-TCW run (a), and its differences (b) between the reference TCW run and no-TCW run. The contour interval is 0.5°C month^{-1} in (a) and 0.1°C month^{-1} in (b).

high-frequency TCW forcing.

3.3 *Processes involved in the remote effects*

Figures 14–15 illustrate examples for model fields simulated from the no-TCW run in July, a month that corresponds to a time when TCs are mostly active over the western tropical Pacific. As is well known (e.g., McCreary and Lu, 1994; Gu and Philander, 1997; Rothstein et al., 1998; Zhang and Liu, 1999), the tropical Pacific Ocean features complicated circulation pathways connecting the extratropics to the tropics, including the subtropical cells (STCs) and the low-latitude western-boundary current pathways. For example, through the western-boundary pathways and the interior North Equatorial Countercurrent (NECC) pathways, off-equatorial waters in the western tropical Pacific converge onto the equator in the central and eastern equatorial Pacific (e.g., Zhang and Busalacchi, 1999; Zhang and Rothstein, 2000; Zhang et al., 1999, 2001). Evidently in Fig. 14 and Fig. 15, the model simulations reveal flow paths that make their connections between the subtropical gyre and the equatorial region in the western Pacific through the low-latitude western boundary currents in the northern (Fig. 15b) and southern Pacific (Fig. 15c), respectively. In particular, the western-boundary pathway in the northern Pacific is well simulated in the OGCM, with a maximum southward flow along 130°E at 10°N (Zhang et al., 1999). In the southern Pacific, the western-boundary pathway is more clearly seen at subsurface depth with a maximum north flow at 155°E (Rothstein et al., 1998). As a result, some subtropical waters flow southward through the western boundary and directly enter into the equatorial region. Over the equator (Fig. 14b), waters in the west transport eastward along the Equatorial Undercurrent (EUC) pathway into the eastern equatorial Pacific. Additionally, the thermocline shoals along the equator from the west to the east (Fig. 14b), indicating that thermal conditions at subsurface depths in the west can affect those at the sea surface in the east.

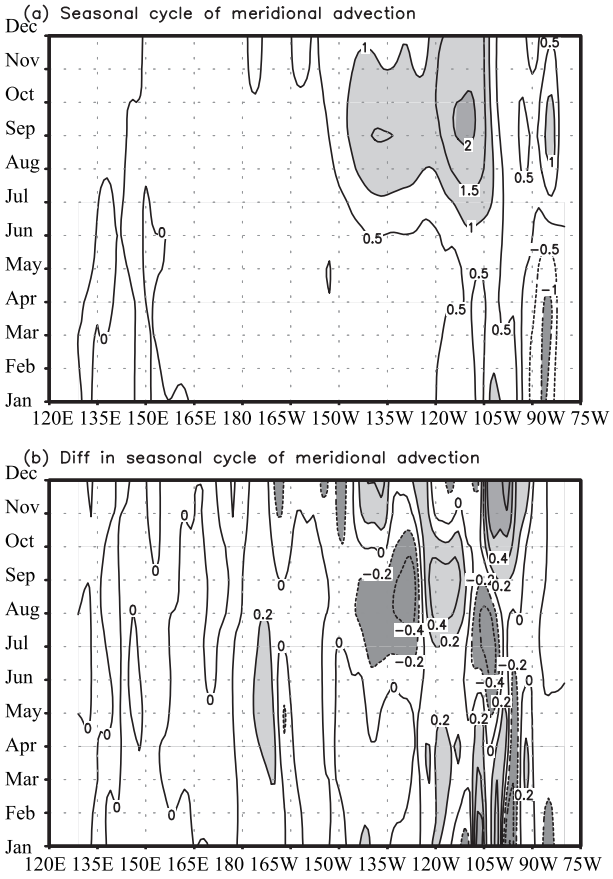

Fig. 12. The same as in Fig. 11 but for the meridional advection term. The contour interval is 0.5°C month^{-1} in (a) and 0.1°C month^{-1} in (b).

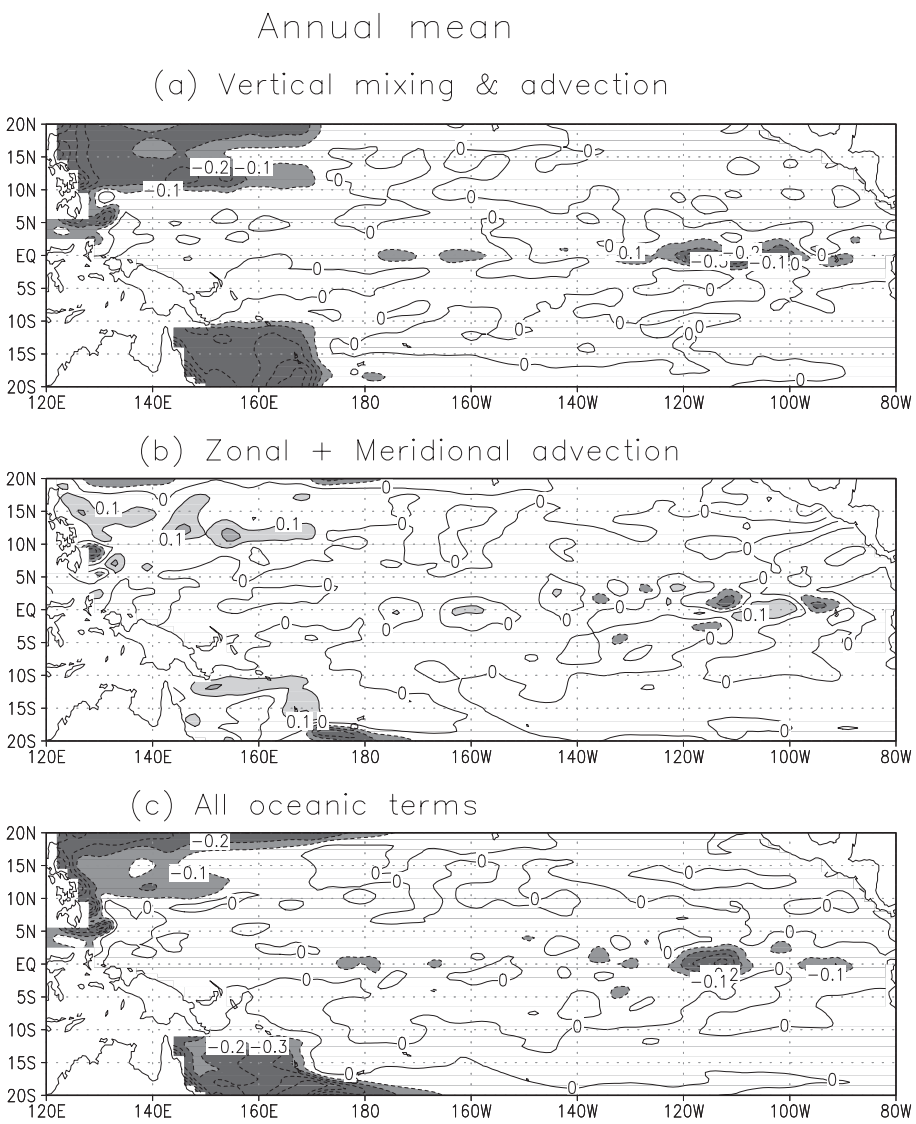

Fig. 13. Horizontal distributions of annual-mean difference fields between the reference TCW run and no-TCW run: the sum of vertical mixing and advection (a), the sum of zonal advection and meridional advection (b), and the sum of all these oceanic budget terms (c), respectively. The contour interval is 0.1°C month^{-1}.

Figure 15a further exhibits an indication of the spreading process of thermal anomalies induced by TCs in the west off the equator into the equatorial region and further into the central-eastern equatorial Pacific. The associated circulation pathways provide a way for thermal anomalies to spread with the mean circulation to the equator through the low-latitude western boundary, which is mostly clearly seen in summer time (from July to August). As such, the gyre circulation brings TC-perturbed waters onto the equator in the western boundary regions and then to the east along the equator, which acts to affect temperature distribution in the eastern equatorial region.

Based on these analyses, Fig. 16 schematically illustrates the processes involved in the remote effects of TCW forcing imposed over the western tropical Pacific on thermal conditions in the east. When seasonally varying TCW forcing is prescribed as a repeated annual cycle over the western Pacific off the equator, large thermal perturbations are induced locally in the ocean, including a cooling in the upper ocean and warming in the thermocline. As these local perturbations persist in the ocean for weeks and longer, they tend to spread with the mean ocean circulation; a pathway can be seen that connects the subtropical gyre, goes through the western boundary currents and extends directly into the equatorial regions and further eastward along the equator. That is, the cooling

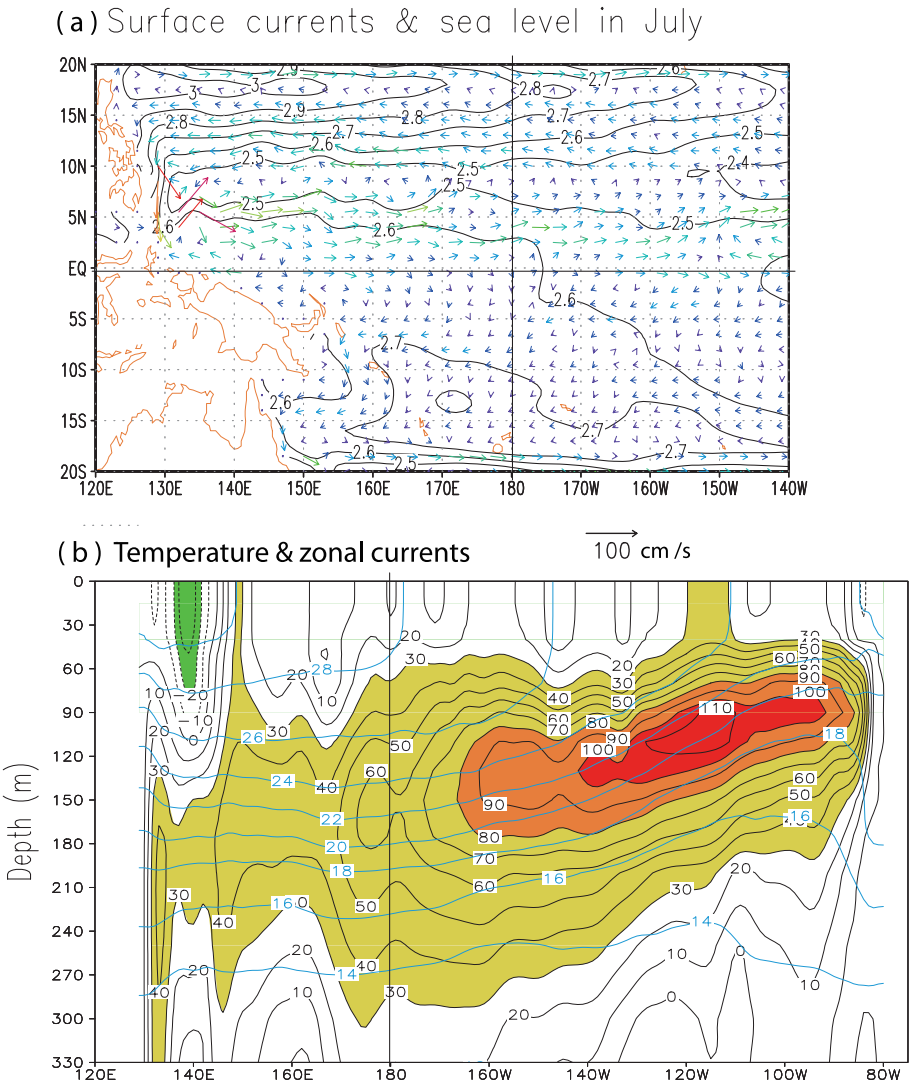

Fig. 14. Fields simulated from the no-TCW run in July for (a) horizontal distributions of dynamical height (contours) and mixed-layer currents (vectors), and (b) zonal-depth section of temperature (the green line) and zonal currents (the black lines with shading) along the equator. The contour interval is 0.1 m for dynamical height in (a), with the current scale unit (the given arrow) being cm s^{-1}; it is 10 cm s^{-1} for the zonal current and 2°C for temperature in (b).

signals in the ML and warming ones in the thermocline in the western tropical Pacific off the equator propagate away from the source regions and spread equatorward through the western-boundary pathways and interior pathways, then through the EUC pathway into the eastern equatorial basin. This produces thermal perturbations in the east that are also characterized by cooling in the ML and warming in the thermocline (e.g., Fig. 6). Furthermore, the locally induced changes in ocean density fields in the east (more dense in the ML but less so in the thermocline) act to weaken the stratification in the vertical and thus destabilize the upper ocean over the eastern equatorial Pacific. These related ocean processes act to enhance the vertical mixing in the upper ocean, leading to the negative SST differences between the TCW run and no-TCW run. As the ocean surface becomes cooling in the TCW run, more heat flux comes into the ocean through the air-sea interface, acting to dampen the negative SST perturbations. In addition, the enhanced vertical mixing tends to displace the thermocline upward, leading to the MLD response that is characterized by a shoaling in the eastern equatorial Pacific.

In short, the well-defined mean water pathways and related thermal structure over the tropical Pacific provide a natural and straightforward way by which

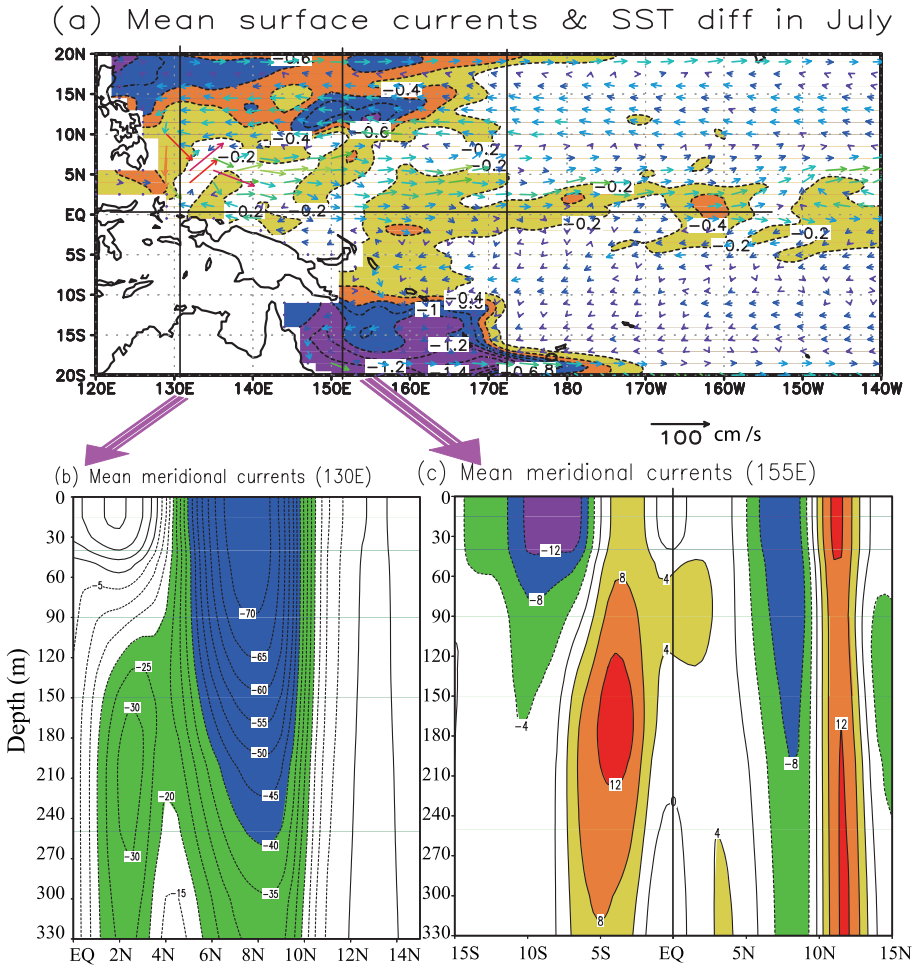

Fig. 15. Fields simulated from the OGCM in July for (a) horizontal distributions of the temperature differences between the TCW and no-TCW runs (contours with shading) and of mixed-layer currents in the no-TCW run (vectors), and for meridional-depth sections of meridional velocity along 130°E (b) and along 155°E (c) in the no-TCW run. The contour interval is 0.2°C for the SST differences in (a), with the current scale unit (the given arrow) being cm s^{-1}; it is 5 cm s^{-1} in (b) and 4 cm s^{-1} in (c).

off-equatorial thermal perturbations induced by TCW forcing in the west can spread equatorward through the low-latitude western boundary currents in the western Pacific, and eastward into the eastern Pacific through the EUC pathways, acting to affect ocean conditions remotely in the east. In particular, SST perturbations induced by TCs off the equator (Fig. 15a) can propagate all the way into the central-eastern equatorial regions. Note that this pathway perspective was also utilized to explain the connections of thermal anomalies off and on the equator in the tropical Pacific during the onset of El Niño events on interannual time scales (e.g., Zhang et al., 1999; Zhang and Rothstein, 2000). In a recent study by Zhang and Wang (2013), this pathway perspective was adopted to explain decadal changes in temperature and salinity fields observed in the western equatorial Pacific in the late 1970s.

4. Sensitivity experiments

Further modeling experiments are performed with different strength and the size of TCW forcing (as represented by α_{TC}, α_x and α_y). Results are quantitatively similar to those illustrated above. Figure 17 presents one example for the temperature differences in the OGCM simulations with α_{TC}=1.0 and α_{TC}=0.0, which can be compared with the results in Fig. 6. As seen, the smaller the values of α_{TC}, the weaker the remote oceanic responses in the eastern

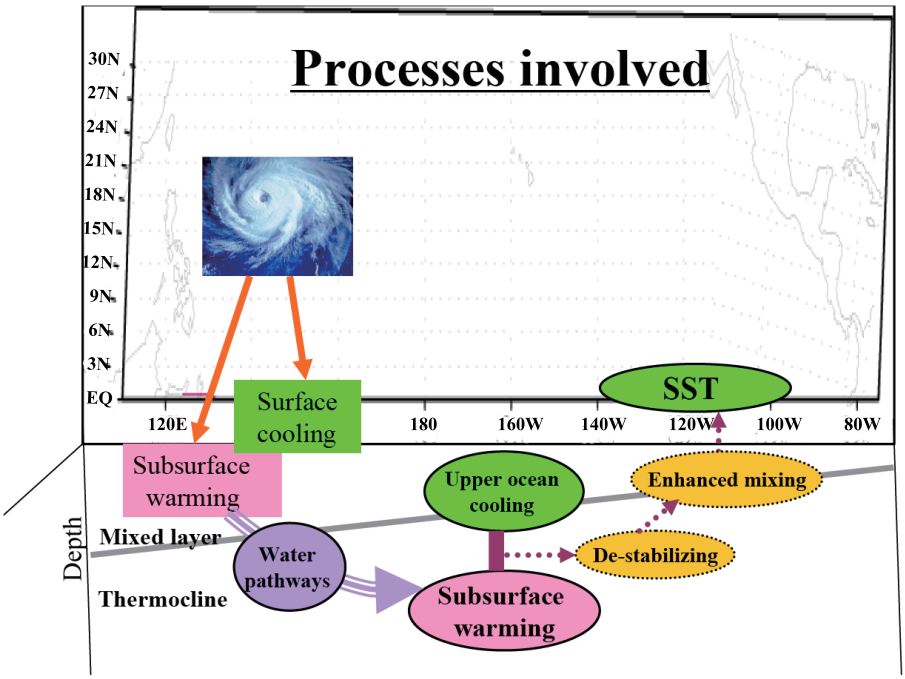

Fig. 16. A schematic diagram showing processes involved in the remote effects of TC-induced wind forcing over the western tropical Pacific on SSTs in the eastern equatorial Pacific. Water pathways in the tropical Pacific provide a mechanism by which thermal perturbations off the equator in the west induced by TCW (i.e., the surface cooling in the ML and subsurface warming beneath the ML in the thermocline) can propagate around the basin, acting to induce thermal responses in the eastern equatorial Pacific. See the main text for details.

equatorial Pacific. In contrast, it is expected that the larger the values of α_{TC}, the stronger the remote oceanic responses in the eastern equatorial Pacific. These results convincingly indicate that the TCW forcing prescribed only over the western tropical Pacific is exerting a remote influence on thermal conditions to the east in a systematic and coherent way, being characterized by a La Niña-like pattern (SST cooling, positive heat flux into the ocean, and shallow ML, respectively). These results clearly indicate that the high-frequency TCW forcing over the western tropical Pacific can affect SSTs in the eastern equatorial Pacific, which is a critically important region to ENSO.

5. Conclusion and discussion

The eastern equatorial Pacific Ocean is the region where the thermocline is shallow, and upwelling and vertical mixing are strongest in the upper ocean, indicating that subsurface thermal perturbations can effectively affect the sea surface. Additionally, the ocean circulation from the western tropical Pacific converges on the equator in this region, providing source waters for the upwelling. These factors indicate that SSTs in the eastern equatorial Pacific can be sensitively affected by remote ocean processes from the west. The western tropical Pacific is a region where TCs are mostly active. Indeed, large perturbations of SST and upper ocean thermal structure are induced locally, which persist for weeks and longer in the region. As the induced perturbations tend to propagate around the basin, they may potentially exert a remote influence on SSTs in the eastern equatorial Pacific. However, the extent to which TCW forcing over the western Pacific can exert a remote influence on thermal conditions in the eastern equatorial Pacific is poorly understood.

In this work, an OGCM is used to examine the remote effects of TC activities over the western tropical Pacific on SSTs in the eastern equatorial Pacific. To isolate TCW forcing effect, the LOESS method is first adopted to explicitly extract TCW structure from six-hour satellite data. It turns out that the LOESS extraction technique can effectively depict TCW forcing patterns (e.g., the structure), but its amplitude and spatial extent can be underestimated. The extracted TCW fields are then explicitly added onto monthly-

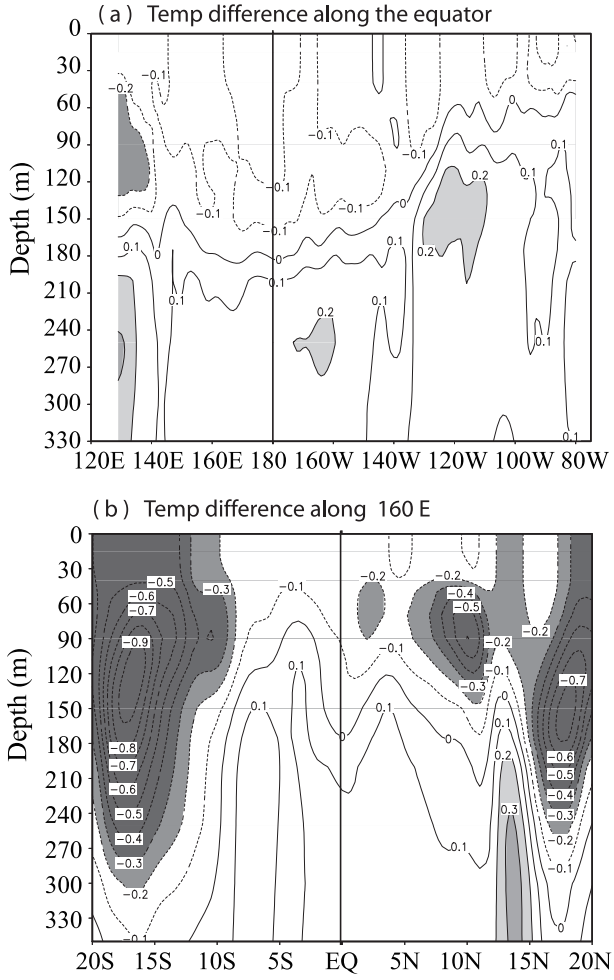

Fig. 17. The same as in Fig. 6 but for a simulation with $\alpha_{\mathrm{TC}} = 1.0$.

mean climatological wind fields to force the OGCM of the tropical Pacific; modeling experiments with and without TCW forcing are performed and compared with each other, allowing a demonstration of its effects on the ocean in a clean and clear way.

When seasonally varying TCW forcing of year 2008 is explicitly imposed only over the western tropical Pacific off the equator, large local effects are found on the ocean, characterized by a cooling in the mixed layer and a warming beneath the mixed layer. Further, the TCW-induced cooling and warming signals locally in the west tend to persist weeks and longer, and to spread with the mean ocean circulation pathways. In particular, a remote oceanic response is seen in the eastern equatorial Pacific, which is also characterized by a cooling in the mixed layer, a warming in the thermocline, and a shoaling of the ML. In addition, when the ocean surface is cooling over the eastern equatorial Pacific in the TCW run, the TCW forcing-induced effects act to increase the sea surface heat flux from the atmosphere to the ocean. This indicates that ocean processes are responsible for the cooling effect on SST. Through the heat budget analyses, it is demonstrated that the colder SSTs seen in the eastern equatorial Pacific in the TCW run are attributed to an enhanced cooling effect from the vertical mixing, accompanied by warming effects from the surface heat flux and meridional advection. As the τ_{TC} part is set zero over the eastern equatorial Pacific, the enhanced vertical mixing effect in the east must be realized through a connection within the ocean.

A pathway perspective is given to attribute the remote effects and explain the results. The tropical Pacific Ocean exhibits complicated circulation structure and water pathways connecting the subtropics to the tropics in the west. For example, through the western-boundary pathways and interior pathways, off-equatorial waters in the western tropical Pacific converge on the equator in the central and eastern equatorial Pacific. Also, the thermocline shoals from the west to east along the equator. These mean circulation pattern and thermal structure over the tropical Pacific provide ways by which thermal perturbations induced by TCs in the west (e.g., signals of the cooling in the ML and the warming beneath the ML) can propagate into the eastern equatorial Pacific. Indeed, a remote effect is seen in the east which is also characterized by cooling in the ML and warming beneath the ML. Furthermore, additional ocean processes are induced locally in the eastern equatorial Pacific. The remotely induced changes in the thermal structure act to modulate vertical density distribution in the east, tending to de-stabilize the stratification and enhance vertical mixing in the upper ocean. These ocean processes induce further SST cooling in the eastern equatorial Pacific in the TCW run relative to the no-TCW run.

These results are considered to be preliminary and obvious limitations exist in these ocean-only modeling efforts. For example, the ocean model used in this paper has a rather coarse horizontal resolution with limited meridional domain. Also, several factors can affect the extent to which TCs exert a remote influence on thermal perturbations in model simulations, including the way TCW forcing is represented. In the modeling results presented in this paper, for instance, the choices of some related parameters characterizing the TCW forcing amplitude and spatial extent (α_{TC}, α_x and α_y) are rather subjective, and the effects simulated in the ocean model are indeed sensitive to these parameters. Although it is expected that the results should be quantitatively the same, there is a clear need to optimize these parameters (i.e., α_{TC}, α_x and α_y) to adequately represent TCW forcing fields.

Clearly, improved TCW forcing representations and ocean modeling tool (e.g., increased horizontal resolution and meridional domain) are necessarily needed to quantify the roles of TCW forcing in remotely modulating thermal structure in the Pacific.

The results from this ocean modeling study could be model-dependent. The Gent-Cane ocean model used here is a layer OGCM, which has a quite different formulation than, say, the National Oceanic and Atmospheric Administration (NOAA)/Geophysical Fluid Dynamics Laboratory Modular Ocean Model (e.g., MOM 3; Pacanowski and Griffies, 1998), which is a level OGCM. For example, in our model, the ML depth and entrainment/detrainment at the base of the ML are determined by a bulk ML model. The vertical mixing, primarily associated with entrainment/detrainment, is estimated from a hybrid mixing scheme (Chen et al., 1994). Since the ML depth in our model is prognostically determined at each time step, all the SST budget terms are simultaneously modulated by the changing depth of the ML. As a result, variations of ML depth can have many ramifications in the SST budget, particularly in controlling the efficiency of mixing and upwelling to cool the SST in the ocean model (Kessler et al., 1998). A comparative modeling study using these differently formulated ocean models (e.g., Zhang et al., 2001) is clearly necessary to fully understand the TCW-induced remote effects on the mean ocean state in the eastern equatorial Pacific.

These ocean-only modeling activities present our first step towards understanding possible feedback of TCs onto ENSO in the tropical Pacific. Further analyses and modeling efforts are underway with improved ocean and coupled ocean-atmosphere models. For example, as indicated in these preliminary modeling experiments, large-scale SSTs in the eastern equatorial Pacific can be modulated by TC-induced wind forcing over the western Pacific. It can be further envisioned that the large-scale SST changes induced by the TCW forcing will feed back onto the climate system of the tropical Pacific. That is, the resultant changes in SST will induce a direct response in the atmosphere; the decrease in SSTs in the eastern equatorial Pacific will increase the east--west temperature contrast along the equator, potentially having effects on large-scale ocean-atmosphere variability in the tropical Pacific associated with ENSO (e.g., Zhang et al., 2013). Also, the induced cooling effect on SST can be a process that makes contributions to observed asymmetry of the two phases of ENSO, El Niño and La Niña. At this stage, all these are speculations and need to be investigated using a coupled ocean-atmosphere model in the near future.

Acknowledgements. We would like to thank A. J. BUSALACCHI, J.-L. SU, and D.-L. ZHANG for their comments, and D. CHELTON and O'NEILL for providing the locally weighted regression (LOESS) code that is utilized for extracting TC wind fields in this work. The author wishes to thank anonymous reviewers for their numerous comments. This research is supported in part by NSF Grant (Grant No. AGS-1061998), NOAA Grant (Grant No. NA08OAR4310885), and NASA Grants (Grant Nos. NNX08AT50G and NNX09AF41G); D. Chen is supported by the National Basic Research Program of China (Grant No. 2013CB430302) and the Public Science and Technology Research Funds of Ocean (Grant No. 201105018); Pei is additionally supported by China Scholarship Council (CSC) with The Ocean University of China, Qingdao, China. The TMI SST data are available from the Remote Sensing Systems website at www.remss.com; the CCMP wind data are available from NASA website at http://podaac.jpl.nasa.gov/.

REFERENCES

Atlas, R., and Coauthors, 2011: A cross-calibrated, multiplatform ocean surface wind velocity product for meteorological and oceanographic applications. *Bull. Amer. Meteor. Soc.*, **92**, 157–174. doi: 10.1175/2010BAMS2946.1.

Camargo, S. J., and A. H. Sobel, 2005: Western North Pacific tropical cyclone intensity and ENSO. *J. Climate,* **18**, 2996–3006.

Camargo, S. J., K. A. Emanuel, and A. H. Sobel, 2007: Use of a genesis potential index to diagnose ENSO effects on tropical cyclone genesis. *J. Climate*, **20**, 4819–4834.

Chan, J. C. L., 1985: Tropical cyclone activity in the northwest Pacific in relation to the El Niño/Southern Oscillation phenomenon. *Mon. Wea. Rev.*, **113**, 599–606.

Chan, J. C. L., 2000: Tropical cyclone activity over the western North Pacific associated with El Niño and La Niña events. *J. Climate*, **13**, 2960–2972.

Chen, D., L. M. Rothstein, and A. J. Busalacchi, 1994: A hybrid vertical mixing scheme and its application to tropical ocean models. *J. Phys. Oceanogr.*, **24**, 2156–2179.

Chen, G., and C. Y. Tam, 2010: Different impacts of two kinds of Pacific Ocean warming on tropical cyclone frequency over the western North Pacific. *Geophys. Res. Lett.*, **37**, L01803, doi: 10.1029/2009GL041708.

Chen, T.-C., S.-Y. Wang, and M.-C. Yen, 2006: Interannual variation of the tropical cyclone activity over the western North Pacific. *J. Climate*, **19**, 5709–5720.

Chia, H.-H., and C. F. Ropelewski, 2002: The interannual variability in the genesis location of tropical cyclones in the northwest Pacific. *J. Climate*, **15**, 2934–2944.

Chu, J.-H., C. R. Sampson, A. S. Levin, and E. Fukada, 2002: The joint typhoon warning center tropical cy-

clone best tracks 1945–2000. Joint Typhoon Warning Center Rep., Pearl Harbor, HI, 22pp.

Elsner, J. B., and K.-B. Liu, 2003: Examining the ENSO–typhoon hypothesis. *Climate Research*, **25**, 43–54.

Emanuel, K. A., 1987: The dependence of hurricane intensity on climate. *Nature*, **326**, 483–485.

Emanuel, K., 2001: Contribution of tropical cyclones to meridional heat transport by the oceans. *J. Geophys. Res.*, **106**, 14771–14781.

Fedorov, A. V., C. M. Brierley, and K. Emanuel, 2010: Tropical cyclones and permanent El Niño in the early Pliocene epoch. *Nature*, **463**, 1066–1070.

Gent, P., and M. A. Cane, 1989: A reduced gravity, primitive equation model of the upper equatorial ocean. *J. Comput. Phys.*, **81**, 444–480.

Ginis, I., 2002: Tropical cyclone–ocean interactions. *Atmosphere–Ocean Interactions*. Vol. **33**, *Advances in Fluid Mechanics Series*, W. Perrie, Ed., WIT Press, 83–114.

Gu, D.-F., and S. G. H. Philander, 1997: Interdecadal climate fluctuations that depend on exchanges between the tropical and extratropics, *Science*, **275**, 805–807.

Hackert, E., A. Busalacchi, and R. Murtugudde, 2001: A wind comparison study using an ocean general circulation model for the 1997–98 El Niño. *J. Geophys. Res.*, **106**, 2345–2362.

Henderson-Sellers, A., and Coauthors, 1998: Tropical cyclones and global climate change: A post-IPCC assessment. *Bull. Amer. Meteor. Soc.*, **79**, 19–38.

Hu, A., and G. A. Meehl, 2009: Effect of the Atlantic hurricanes on the oceanic meridional overturning circulation and heat transport. *Geophys. Res. Lett.*, **36**, L03702, doi: 10.1029/2008GL036680.

Huang, P., T. B. Sanford, and J. Imberger, 2009: Heat and turbulent kinetic energy budgets for surface layer cooling induced by the passage of Hurricane Frances (2004). *J. Geophys. Res.*, **114**, C12023, doi: 10.1029/2009JC005603.

Irwin, R. P., and R. E. Davis, 1999: The relationship between the Southern Oscillation Index and tropical cyclone tracks in the eastern North Pacific. *Geophys. Res. Lett.*, **20**, 2251–2254.

Jacob, S. D., L. K. Shay, and A. J. Mariano, 2000: The 3D oceanic mixed layer response to hurricane Gilbert. *J. Phys. Oceanogr.*, **30**, 1407–1429.

Jansen, M., and R. Ferrari, 2009: Impact of the latitudinal distribution of tropical cyclones on ocean heat transport. *Geophys. Res. Lett.*, **36**, L06604, doi: 10.1029/2008GL036796.

Kessler, W. S., L. M. Rothstein, and D. Chen, 1998: The annual cycle of SST in the eastern tropical Pacific, diagnosed in an ocean GCM. *J. Climate*, **11**, 777–799.

Kim, H.-M., P. J. Webster, and J. A. Curry, 2011: Modulation of North Pacific tropical cyclone activity by three phases of ENSO. *J. Climate*, **24**, 1839–1849, doi: 10.1175/2010JCLI3939.1

Korty, R. L., K. Emanuel, and J. R. Scott, 2008: Tropical cyclone–induced upper-ocean mixing and climate: Application to equable climates. *J. Climate*, **21**, 638–654.

Levitus, S., J. I. Antonov, and T. P. Boyer, 2005: Warming of the world ocean, 1955–2003. *Geophys. Res. Lett.*, **32**, L02604, doi: 10.1029GL021592.

Lin, I.-I., W. T. Liu, C.-C. Wu, J. C. H. Chiang, and C.-H. Sui, 2003: Satellite observations of modulation of surface winds by typhoon-induced upper ocean cooling. *Geophys. Res. Lett.*, **30**, 1131, doi: 10.1029/2002GL015674.

McCreary, J. P., and P. Lu, 1994: Interaction between the subtropical and equatorial ocean circulations: The subtropical gyre, *J. Phys. Oceanogr.*, **24**, 466–497.

Monterey, G. I., and S. Levitus, 1997: Seasonal variability of mixed layer depth for the World Ocean. NOAA NESDIS Atlas 14, 100pp.

Murtugudde, R., and A. J. Busalacchi, 1998: Salinity effects in a tropical ocean model. *J. Geophys. Res.*, **103**, 3283–3300.

Murtugudde, R., R. Seager, and A. J. Busalacchi, 1996: Simulation of tropical oceans with an ocean GCM coupled to an atmospheric mixed layer model. *J. Climate*, **9**, 1795–1815.

Murtugudde, R., J. Beauchamp, C. R. McClain, M. Lewis, and A. J. Busalacchi, 2002: Effects of penetrative radiation on the upper tropical ocean circulation. *J. Climate*. **15**, 470–486.

O'Neill, L.W., D. B. Chelton, and S. K. Esbensen, 2010: The effects of SST-induced surface wind speed and direction gradients on midlatitude surface vorticity and divergence. *J. Climate*, **23**, 255–281.

Pacanowski, R. C., and S. M. Griffies, 1998: MOM 3.0 Manual. NOAA/Geophysical Fluid Dynamics Laboratory, 700pp. [Available online at http://www.ocgy.ubc.ca/∼yzq/books/MOM3/guide_parent.html.]

Pasquero, C., and K. Emanuel, 2008: Tropical cyclones and transient upper ocean warming. *J. Climate*, **21**, 129–141.

Price, J. F., 1981: Upper ocean response to a hurricane. *J. Phys. Oceanogr.*, **11**, 153–175.

Price, J. F., J. Morzel, and P. P. Niiler, 2008: Warming of SST in the cool wake of a moving hurricane. *J. Geophys. Res.*, **113**, C07010, doi: 10.1029/2007JC004393.

Rothstein, L. M., R.-H. Zhang, A. J. Busalacchi, and D. Chen, 1998: A numerical simulation of the mean water pathways in the subtropical and tropical Pacific Ocean. *J. Phys. Oceanogr.*, **28**, 322–343.

Seager, R., M. Blumenthal, and Y. Kushinir, 1995: An advective atmospheric mixed layer model for ocean modeling purposes: Global simulation of surface heat fluxes. *J. Climate*, **8**, 1951–1964.

Sriver, R. L., and M. Huber, 2007: Observational evidence for an ocean heat pump induced by tropical cyclones. *Nature*, **447**, 557–580.

Sriver, R. L., and M. Huber, 2010: Modeled sensitivity of upper thermocline properties to tropical cyclone winds and possible feedbacks on the Hadley circulation. *Geophys. Res. Lett.*, **37**, L08704, doi:

10.1029/2010GL042836.

Sriver, R. L., M. Goes, M. E. Mann, and K. Keller, 2010: Climate response to tropical cyclone-induced ocean mixing in an Earth system model of intermediate complexity. *J. Geophys. Res.*, **115**, C10042, doi: 10.1029/2010JC006106.

Vincent, E. M., M. Lengaigne, G. Madec, J. Vialard, G. Samson, N. C. Jourdain, C. E. Menkes, and S. Jullien, 2012: Processes setting the characteristics of sea surface cooling induced by tropical cyclones. *J. Geophys. Res.*, **117**, C02020, doi: 10.1029/2011JC007396.

Wang, B., and J. C. L. Chan, 2002: How strong ENSO events affect tropical storm activity over the western North Pacific. *J. Climate*, **15**, 1643–1658.

Webster, P. J., G. J. Holland, J. A. Curry, and H.-R. Chang, 2005: Changes in tropical cyclone number, duration and intensity in a warming environment. *Science*, **309**, 1844–1846.

Wentz, F. J., C. Gentemann, D. Smith, and D. Chelton, 2000: Satellite measurements of sea surface temperature through clouds. *Science*, **288**, 847–850.

Xie, P., and P. Arkin, 1995: An intercomparison of gauge observations and satellite estimates of monthly precipitation. *J. Appl. Meteor.*, **34**, 1143–1160.

Zedler, S. E., 2009: Simulations of the ocean response to a hurricane: Nonlinear processes. *J. Phys. Oceanogr.*, **39**, 2618–2634.

Zhang, R.-H., and A. J. Busalacchi, 1999: A possible link between off-equatorial warm anomalies propagating along the NECC path and the onset of the 1997–98 El Niño. *Geophys. Res. Lett.*, **26**, 2873–2876.

Zhang, R.-H., and Z. Liu, 1999: Decadal thermocline variability in the North Pacific Ocean: Two anomaly pathways around the Subtropical Gyre. *J. Climate*, **12**, 3273–3296.

Zhang, R.-H., and L. M. Rothstein, 2000: Role of off-equatorial subsurface anomalies in initiating the 1991–1992 El Niño as revealed by the National Centers for Environmental Prediction ocean reanalysis data. *J. Geophys. Res.*, **105C**, 6327–6339, doi: 10.1029/1999JC900316.

Zhang, R.-H., and A. J. Busalacchi, 2008: Rectified effects of tropical instability wave (TIW)-induced atmospheric wind feedback in the tropical Pacific. *Geophys. Res. Lett.*, **35**, L05608, doi: 10.1029/2007GL033028.

Zhang, R.-H., and A. J. Busalacchi, 2009: Freshwater flux (FWF)-induced oceanic feedback in a hybrid coupled model of the tropical Pacific. *J. Climate*, **22**(4), 853–879.

Zhang, R.-H., and Z. G. Wang, 2013: Model evidence for interdecadal pathway changes in the subtropics and tropics of the South Pacific Ocean. *Adv. Atmos. Sci.*, **30**, 1–9, doi: 10.1007/s00376-012-2048-1.

Zhang, R.-H., L. M. Rothstein, A. J. Busalacchi, and X. Z. Liang, 1999: The onset of the 1991–92 El Niño event in the tropical pacific ocean: The NECC subsurface pathway. *Geophys. Res. Lett.*, **26**, 847–850.

Zhang, R.-H., T. Takashi, and S. E. Zebiak, 2001: Subduction of decadal North Pacific thermal anomalies in an ocean GCM. *Geophys. Res. Lett.*, **28**, 2449–2452.

Zhang, R.-H., A. J. Busalacchi, and R. G. Murtugudde, 2006: Improving SST anomaly simulations in a layer ocean model with an embedded entrainment temperature submodel. *J. Climate*, **19**, 4638–4663.

Zhang, R.-H., A. J. Busalacchi, X. Wang, J. Ballabrera-Poy, R. G. Murtugudde, E. C. Hackert, and D. Chen, 2009: Role of ocean biology-induced climate feedback in the modulation of El Niño-Southern Oscillation. *Geophys. Res. Lett.*, **36**, L03608, doi: 10.1029/2008GL036568.

Zhang, R.-H., F. Zheng, J. Zhu, Y. H. Pei, Q. Zheng, and Z. G. Wang, 2012: Modulation of El Niño-Southern Oscillation by freshwater flux and salinity variability in the tropical Pacific. *Adv. Atmos. Sci.*, **29**, 647–660, doi: 10.1007/s00376-012-1235-4.

Zhang, R.-H., F. Zheng, J. Zhu, and Z. G. Wang, 2013: A successful real-time forecast of the 2010–11 La Niña event. *Sci. Rep.*, **3**, 1108, doi: 10.1038/srep01108.